


# The influence of elevated $\text{SiO}_2(aq)$ on intracellular silica uptake and microbial metabolism

Rosalie Tostevin<sup>1,2</sup>  | Joseph T. Snow<sup>2</sup> | Qiong Zhang<sup>2</sup> | Nicholas J. Tosca<sup>2</sup> | Rosalind E.M. Rickaby<sup>2</sup>

<sup>1</sup>Department of Geological Sciences, University of Cape Town, Cape Town, South Africa

<sup>2</sup>Department of Earth Science, University of Oxford, Oxford, UK

## Correspondence

Rosalie Tostevin, Department of Geological Sciences, University of Cape Town, Rondebosch, Cape Town 7701, South Africa.  
Email: Rosalie.tostevin@uct.ac.za.

## Funding information

NRF BIOGRIP platform; NRF-DSI COE Palaeoscience; APPELS, Grant/Award Number: 681746; NERC, Grant/Award Number: NE/M013014/1

## Abstract

Microbes are known to accumulate intracellular  $\text{SiO}_2(aq)$  up to 100s of mmol/l from modern seawater ( $\text{SiO}_2(aq) < 100 \mu\text{mol/l}$ ), despite having no known nutrient requirement for Si. Before the evolution of siliceous skeletons, marine silica concentrations were likely an order of magnitude higher than the modern ocean, raising the possibility that intracellular  $\text{SiO}_2(aq)$  accumulation interfered with normal cellular function in non-silicifying algae. Yet, because few culturing studies have isolated the effects of  $\text{SiO}_2(aq)$  at high concentration, the potential impact of elevated marine silica on early microbial evolution is unknown. Here, we test the influence of elevated  $\text{SiO}_2(aq)$  on eukaryotic algae, as well as a prokaryote species. Our results demonstrate that under  $\text{SiO}_2(aq)$  concentrations relevant to ancient seawater, intracellular Si accumulates to concentrations comparable to those found in siliceous algae such as diatoms. In addition, all eukaryotic algae showed a statistically significant response to the high-Si treatment, including reduced average cell sizes and/or a reduction in the maximum growth rate. In contrast, there was no consistent response to the high-Si treatment by the prokaryote species. Our results highlight the possibility that elevated marine  $\text{SiO}_2(aq)$  may have been an environmental stressor during early eukaryotic evolution.

## KEYWORDS

Archaeal, culturing, microbial metabolism, Proterozoic, silica

## 1 | INTRODUCTION

The sedimentary record indicates that marine dissolved silica concentrations declined dramatically from the Precambrian (>541 million years ago, Ma) and through the Phanerozoic. For example, syndepositional and early diagenetic microcrystalline quartz (or chert) is essentially ubiquitous in peritidal sedimentary deposits spanning most of the Precambrian (Maliva et al., 1989, 2005). In addition, Archaeal sedimentary successions preserve petrographic evidence for primary silica precipitation and sedimentation on continental margins and in deeper basinal settings (Figure 1) (Rasmussen et al., 2015; Stefurak et al., 2015). Collectively, these observations indicate that global average  $\text{SiO}_2(aq)$  may have been poised as high

as cristobalite or amorphous silica saturation, corresponding to concentrations between 0.67 and 2.2 mmol/L (Siever, 1992; Siever & Woodford, 1973). The postulated Neoproterozoic origins of siliceous sponges, and their later Cambrian radiation, may have driven a modest decrease in marine  $\text{SiO}_2$  levels, but early diagenetic chert remains a dominant component throughout much of the Palaeozoic Era (Figure 1) (Brocks et al., 2017; Conley et al., 2017; Kidder & Mumma, 2003; Sperling et al., 2010). Siliceous radiolarians appeared in the Cambrian, but only diversified and became environmentally significant in the Triassic, and may have further lowered marine silica concentrations (Conley et al., 2017; Wever et al., 2003). Subsequently, siliceous diatoms appeared in the Mesozoic, and their widespread Cenozoic expansion, particularly in the Southern Ocean

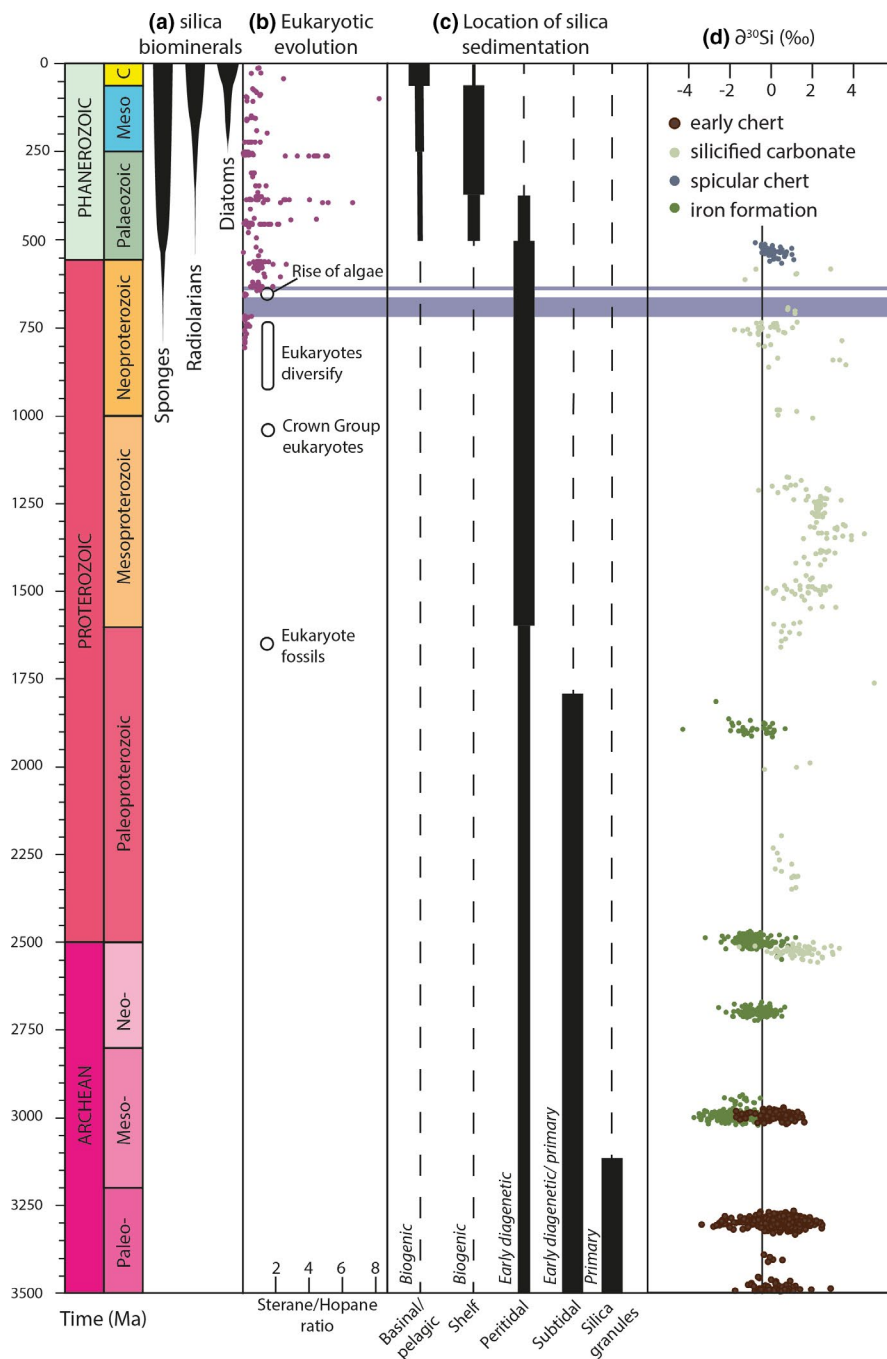


**FIGURE 1** (a) Summary of the evolution of siliceous organisms, where the width of the black lines indicates relative abundance through time. (b) Sterane-to-hopane ratios from Brocks et al. (2017), indicating the ecological contribution of eukaryotes/prokaryotes to sedimentary organic carbon (purple circles) and key events in early eukaryotic evolution (open circles). (c) Changes in the dominant location of silica sedimentation through time, where the width of the bar represents the relative importance of the sink (Maliva et al., 2005). (d)  $\delta^{30}\text{Si}$  data from Trower and Fischer (2019), from iron formation (dark green), spicular chert (blue), silicified carbonate (light green) and early chert (dark brown) compared with bulk silicate Earth (black line)

across the Eocene–Oligocene boundary (Egan et al., 2013), is commonly thought to have decreased marine silica concentrations to modern levels ( $<100 \mu\text{mol/L}$  in deep water) and shifted the locus of siliceous sedimentation to basinal settings (Sims et al., 2006).

Although  $\text{SiO}_2$  was a major constituent of seawater for much of Earth's history, the impact of high silica concentrations on non-silicifying microbes is poorly constrained. Silica is not considered an essential nutrient for non-silicifying microbes, and many species can grow in media with no added silica. However, prokaryotes and eukaryotes clearly evolved and diversified in oceans with dramatically different  $\text{SiO}_2$  compared with today. The presence of elevated  $\text{SiO}_2$  may influence non-silicifying microbes in several ways. For example, if silica accumulates inside the cell, microbes may be unequipped

to manage high intracellular  $\text{SiO}_2$  levels. In addition,  $\text{SiO}_2(\text{aq})$  forms aqueous complexes with other dissolved species, which may alter their bioavailability in seawater and potentially also inside the cell, resulting in nutrient limitation. In addition, silica may also be taken up through ion-specific channels designed for chemically similar species, blocking nutrients from entering the cell (Wu & Beitz, 2007). However, if extant species have a genetic memory of ancient high- $\text{SiO}_2$  oceans, they may have cellular machinery to circumvent these potential issues (Marron et al., 2016).

Although previous work has examined the impacts of aqueous silica concentrations on phytoplankton in the range  $1\text{--}100 \mu\text{mol/L}$  (Baines et al., 2012; Brzezinski et al., 2017; Fuhrman et al., 1978), those studies did not extend to the very high silica concentrations

thought to be relevant to the Precambrian oceans. Thus, to evaluate responses of major eukaryotic lineages to  $\text{SiO}_2$  addition at high concentration, we grew three chlorophyll *a* + *c*-containing algae ("red lineage") and one chlorophyll *a* + *b*-containing algae ("green lineage"), including calcifying and non-calcifying strains, under variable  $\text{SiO}_2$  (up to 2.1 mmol/L). We analysed two key functional traits, cell size and growth rates, as well as cellular quotas of phosphorus, silica and a range of bioessential metals. For comparison with the prokaryotic realm, we also investigated a cyanobacteria species known to accumulate intracellular silica.

## 2 | METHODS

### 2.1 | Microbe species

All culture strains were acquired from the Roscoff Culture collection (Roscoff, France). Eukaryote species selected for the study included three chlorophyll *a* + *c*-containing algae, *Thoracosphaera heimii* (strain RCC 1512), *Pavlova lutheri* (strain RCC 1547) and *Emiliania huxleyi* (strain RCC 1216). Since these strains all acquired their plastids via secondary endosymbiosis from red algae (rhodophytes), they will be referred to hereafter as red lineage. In addition, we selected one chlorophyll *a* + *b*-containing algae (hereafter green lineage), *Chlamydomonas concordia* (strain RCC 1), and one prokaryote species, *Synechococcus* sp. (strain WH8102/RCC539). The selected group includes species that possess silica transporters, such as SITs, SIT-Ls and Lsi2, and others that do not. *T. heimii* is a calcifying dinoflagellate and member of the Alveolata division. There is no genome available for *T. heimii*, but other dinoflagellates have SIT-2 and Lsi2-like transporters (Marron et al., 2016). *E. huxleyi* is a calcifying coccolithophore and a member of the Haptophyta division. Some coccolithophore species have SITs, and *E. huxleyi* has Lsi2-like transporters (Durak et al., 2016). *P. lutheri* is a non-calcifying red lineage algae and member of the Haptophyta division and has no reported Si transporters. *C. concordia* is a non-calcifying algae from the green lineage and member of the division chlorophyta. The presence of Si transporters in *C. concordia* is not documented, but closely related *C. reinhardtii* has none. *Synechococcus* is a globally abundant cyanobacteria previously shown to accumulate intracellular Si and contains SIT-L genes (Baines et al., 2012; Brzezinski et al., 2017).

### 2.2 | Culture conditions

Each species was grown as a batch culture in an artificial seawater media, Aquil\* (Price et al., 1989; Sunda et al., 2005). Aquil\* is enriched with 100  $\mu\text{mol/L}$  nitrate and 10  $\mu\text{mol/L}$  phosphate, and in equilibrium with modern atmospheric  $\text{CO}_2$ . In the control, silicic acid was not added, but unamended concentrations ranged up to 25  $\mu\text{M}$  due to the presence of trace amounts of silica in other salts (Media A, Table 1). In silica-rich seawater,  $\text{SiO}_2$  was added to achieve concentrations ranging between 1.2 and 2.1 mmol/L from sodium

**TABLE 1**  $\text{SiO}_2(\text{aq})$  concentrations in each batch of media, analysed via ICP-OES. Average error is <5% ( $1\sigma$ )

Media type	$\text{SiO}_2(\text{aq})$
A	<25 $\mu\text{mol/L}$
B	0.1 mmol/L
C	1.2 mmol/L
D	1.6 mmol/L
E	2.1 mmol/L

metasilicate stock solutions (media C–E, Table 1).  $\text{SiO}_2$  was added before any nutrients and stirred for >48 hr to ensure the stock solution was fully equilibrated with the media.  $\text{SiO}_2$  was varied between batches of media to test whether there was a progressive response to increases in  $\text{SiO}_2$ . Si concentrations in each batch of media were analysed via inductively coupled plasma optical emission spectroscopy (ICP-OES) at the University of Cambridge. Vitamins and trace metals were added according to the Aquil\* recipe (Price et al., 1989; Sunda et al., 2005). The media was pH balanced to 8.1–8.2 prior to inoculation by the addition of NaOH and HCl. The trace metal chelator EDTA (ethylenediaminetetraacetic acid) was added to the trace metal stock solutions to guarantee a constant level of bioavailable metals and prevent metal precipitation. All stock solutions were added under sterile conditions in a laminar flow hood.

All culture bottles were manually and carefully rotated daily to avoid cell settling. The cultures were incubated in a climate chamber at a constant temperature of 15°C for haptophyta and alveolata, and 20°C for dinoflagellates and cyanobacteria, at a 12:12 (hour:hour) light-dark cycle and at a photon flux density of 20  $\mu\text{mol photons m}^{-2} \text{s}^{-1}$  for alveolata and haptophyta and 100  $\mu\text{mol photons m}^{-2} \text{s}^{-1}$  for dinoflagellates and cyanobacteria. All cultures were grown in sterile non-TC-treated 100-cm<sup>3</sup> polystyrene culture vessels. All work was undertaken using sterile techniques, and cultures were only opened inside a sterile laminar flow hood and sampled with autoclaved pipette tips. The initial cell density was low, and cells were transferred into fresh media during mid-exponential phase. Each species was grown in triplicate under both silica-rich and control conditions. Some cultures were also grown under standard Aquil\* media, with 100  $\mu\text{M}$  of added  $\text{SiO}_2$  (Media B, Table 1). The pH of the media was monitored during exponential growth of both *T. heimii* and *E. huxleyi* in silica-rich media as well as a sterile control.

### 2.3 | Cell abundance and growth rate

Samples for cell abundance were taken at regular intervals throughout lag, exponential and early stationary phase. Care was taken to sample within the same time interval each day, and control and Si-rich conditions were sampled within five minutes of each other. Incubation bottles were agitated to obtain a homogeneous suspension of cells before sampling. Eukaryote cells were diluted 10-fold with a 3.5% NaCl solution and immediately measured in triplicate using a Beckman Z1 Coulter counter within a species-specific size

window designed to exclude debris, such as dead cells, bacteria or detached coccoliths. The Coulter counter was calibrated using spherical beads. Species-specific daily growth rates were calculated from the least-squares regression of cell counts versus time during exponential growth (Eq).

$$\mu = [\ln(c_1) - \ln(c_0)] / [t_1 - t_0]$$

where  $c_0$  and  $c_1$  are the cell concentrations at the beginning ( $t_0$ ) and end ( $t_1$ ) of the incubation period (for full cell count and cell size data, see Figures S1–S5). The optimal period for calculating exponential growth was carefully assessed for each sub-culture, ensuring that the points used remained within the exponential growth phase, covered several complete photoperiods and excluded data points associated with large error bars (Figures S1–S5). Growth rates in this study refer to cell division rates, rather than increased cellular mass. The spherical equivalent diameter of cells was also measured using a coulter counter and used to calculate the mean diameter. *T. heimii* and *E. huxleyi* samples were acidified with a few drops of 10 M HCl after analysis, mixed for one hour and reanalysed to determine naked cell size after dissolution of calcified shells.

Chlorophyll levels in cyanobacteria cultures were measured in triplicate using a TECAN spark® Multimode plate reader at an excitation wavelength of 485 nm. Chlorophyll levels can be assumed to track cell density but may also be influenced by variations in the pigment content of individual cells within each treatment. For all species, analysis was performed within a one-hour time window daily to minimise the influence of sampling different parts of the daily growth cycles.

## 2.4 | Cell imaging

Samples were taken from the *T. heimii* incubation bottles, and 2 ml of media was filtered under low vacuum onto polycarbonate filters (0.22 µm pore size) and rinsed five times with 10 mmol/L CaCl<sub>2</sub> and then five times with 100% ethanol. Filter papers were dried in a laminar flow hood. Samples were gold-coated, and SEM analysis was performed at the Dunn School of Bioimaging in the Department of Physiology, University of Oxford with a Zeiss Sigma 300 FEG-SEM.

## 2.5 | Total digestions

Cells were centrifuged during mid-exponential phase and washed three times in chelexed metal-free seawater, which had a pH of 8 and contained no added nutrients or Si (SOW). During each wash, the cells were in contact with the SOW for over 20 min. Cells were then dried under laminar flow and frozen for >24 hr. Cell pellets were transferred to clean Teflon beakers under clean laboratory ISO 100 conditions and digested in a 4:6 mixture of hydrogen peroxide and concentrated nitric acid under reflux for 24 hr. The digests were then dried down and re-suspended in 2% nitric acid for analysis via flow

injection ICP-MS (Qiong Zhang et al., 2018). The concentration of metals in the media was also analysed via ICP-MS. Si was measured on the same digests via ICP-OES at the University of Cambridge. Cellular element concentrations were calculated based on the total number of cells and the average cell volume, as measured on a Coulter counter (See section 2.3). These bulk cellular digests reflect intracellular concentrations but will also include contributions from any species precipitated on or adsorbed to the exterior cell wall.

## 3 | RESULTS

### 3.1 | Growth rates and cell diameter

Consistently reduced growth rates were observed in *T. heimii*, *C. concordia* and *P. lutheri* in silica-rich seawater compared with the control (Figure 2). These differences were statistically significant as determined by a one-way ANOVA test (Figure S6 and table 2). In contrast, there was no consistent difference in growth rate for *E. huxleyi* or *Synechococcus sp.* between the high-silica treatment (Media C–E) and the control (Media A, no added SiO<sub>2</sub>) (Figure 2). For algae grown under intermediate-SiO<sub>2</sub> seawater (Media B = 100 µmol/L SiO<sub>2</sub>), there was no significant difference in growth rates compared with the control (Media A). The pH remained within error of sterile media during early and mid-exponential phase but started to rise in late exponential phase once cell densities reached >10<sup>5</sup> per ml, reaching 8.4 by stationary phase (Figure S7).

Another striking difference between the high-Si treatment (Media C–E) and the control (Media A) was reduced average cell diameter at maximum growth rates, observed in *T. heimii*, *E. huxleyi* and *P. lutheri* (at the  $p < .05$  level, see Figure 2 and table 2). The cell size difference persisted in *T. heimii* and *E. huxleyi* after acidification, suggesting a true difference in the size of the naked cell, rather than a change in calcification (see Figure S8). The reduced diameter translates into a dramatically reduced surface area and cell volume but increases the surface area-to-volume ratio. There was no consistent difference in cell diameter observed in *C. concordia*, and no cell size data are available for *Synechococcus sp.* In summary, all species showed a systematic response to elevated SiO<sub>2</sub>, via reduced growth rates and/or cell size, except for the prokaryote species, *Synechococcus sp.*

### 3.2 | Cellular composition

In general, eukaryotic metal quotas for Fe, Mn, Br and Zn are high compared with Co, Cd, Cu, I, Mo, Zr, Ba, Cr and Se, in agreement with the less expansive previous cellular metal quotas reported in Quigg et al. (2003) (see supplementary discussion). There is a small but progressive increase in the intracellular concentration of Se, Mo and Ba at higher silica concentrations for *T. heimii* (Figure 3), and a larger increase in the concentration of intracellular As, Al and Zr. Similarly, the cellular concentration of Mo, Ba, Al and As is

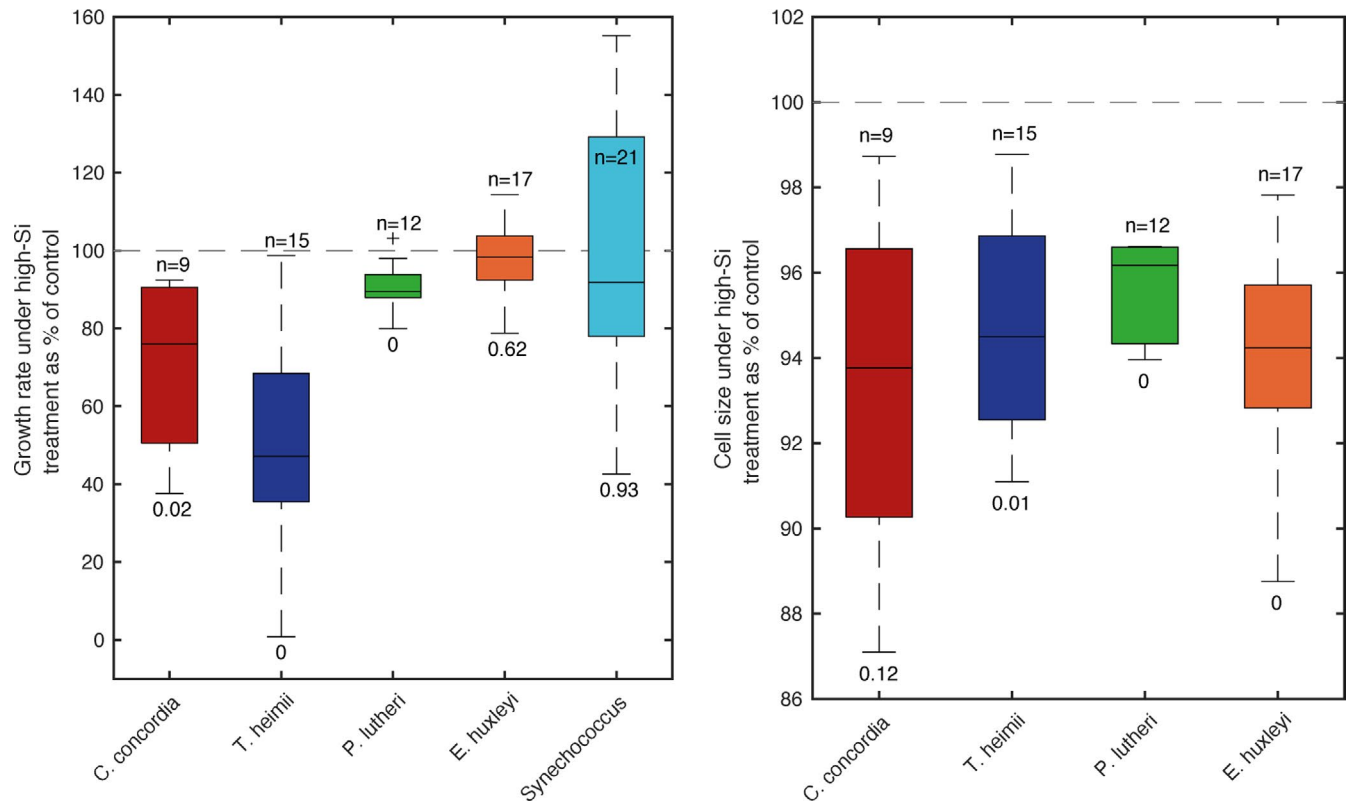


**FIGURE 2** Box plots showing the maximum growth rates (left) and cell size at maximum growth rates (right) for the high-Si treatment as a percentage of the control. The black cross indicates an outlier. The result was calculated independently for “n” independent replicate cultures (plus an equivalent number of control cultures). The values below the bars are P-values for one-way ANOVA tests, rounded to two decimal digits (i.e. values of 0 represent  $p < .005$ ). P-values  $< 0.05$  are interpreted to indicate that the means of the two groups are significantly different. *C. concordia*, *T. heimii* and *P. lutheri* show reduced growth rates, and *C. concordia*, *T. heimii* and *E. huxleyi* show reduced cell size

**TABLE 2** Average growth rates and cell size at maximum growth rate for Si-rich and control experiments across all sub-cultures

Species	Mean growth rate			Mean cell size		
	High-Si	Control	One-way ANOVA test	High-Si	Control	One-way ANOVA test
<i>C. concordia</i>	$0.15 \pm 0.05$	$0.20 \pm 0.04$	$F(1,16) = 6.72$ , $p = .02$	$5.56 \pm 0.57$	$5.94 \pm 0.41$	$F(1,16) = 2.67$ , $p = .12$
<i>T. heimii</i>	$0.31 \pm 0.18$	$0.58 \pm 0.26$	$F(1,28) = 11.28$ , $p = .00$	$10.42 \pm 0.53$	$11.02 \pm 0.58$	$F(1,28) = 8.89$ , $p = .01$
<i>P. lutheri</i>	$0.16 \pm 0.03$	$0.17 \pm 0.03$	$F(1,10) = 82.93$ , $p = .00$	$4.48 \pm 0.04$	$4.68 \pm 0.07$	$F(1,10) = 42.44$ , $p = .00$
<i>E. huxleyi</i>	$0.76 \pm 0.11$	$0.78 \pm 0.12$	$F(1,52) = 0.25$ , $p = .62$	$4.81 \pm 0.18$	$5.10 \pm 0.16$	$F(1,52) = 42.21$ , $p = .00$
<i>Synechococcus</i> sp.	$0.31 \pm 0.22$	$0.30 \pm 0.20$	$F(1,40) = 0.01$ , $p = .93$	N/A	N/A	N/A

Note: Error is one standard deviation. Results of one-way ANOVA test for high-silica treatments compared with control for each sub-culture.  $p < .05$  suggests the difference between the means of the two groups is statistically significant. The F statistic [F(B,W) = R] states the degrees of freedom between (B) and within (W) each group, respectively, which is used to calculate the F ratio (R).

significantly higher in *C. concordia* cells grown in silica-rich seawater compared with a control (Figure 3). For *P. lutheri*, the cellular concentration of Al and Ge is higher in silica-rich conditions compared to the control (Figure 3). Other metals show no change outside of error (1 SD) between the control and silica-rich conditions. These

patterns cannot be explained by different concentrations of metal in the sterile media (see Figure S9 in the supplementary information). In summary, for most bioessential metals, elevated  $\text{SiO}_2(aq)$  does not appear to influence cellular metal quotas, but there is an increase in the intracellular concentration of some toxic metalloids.

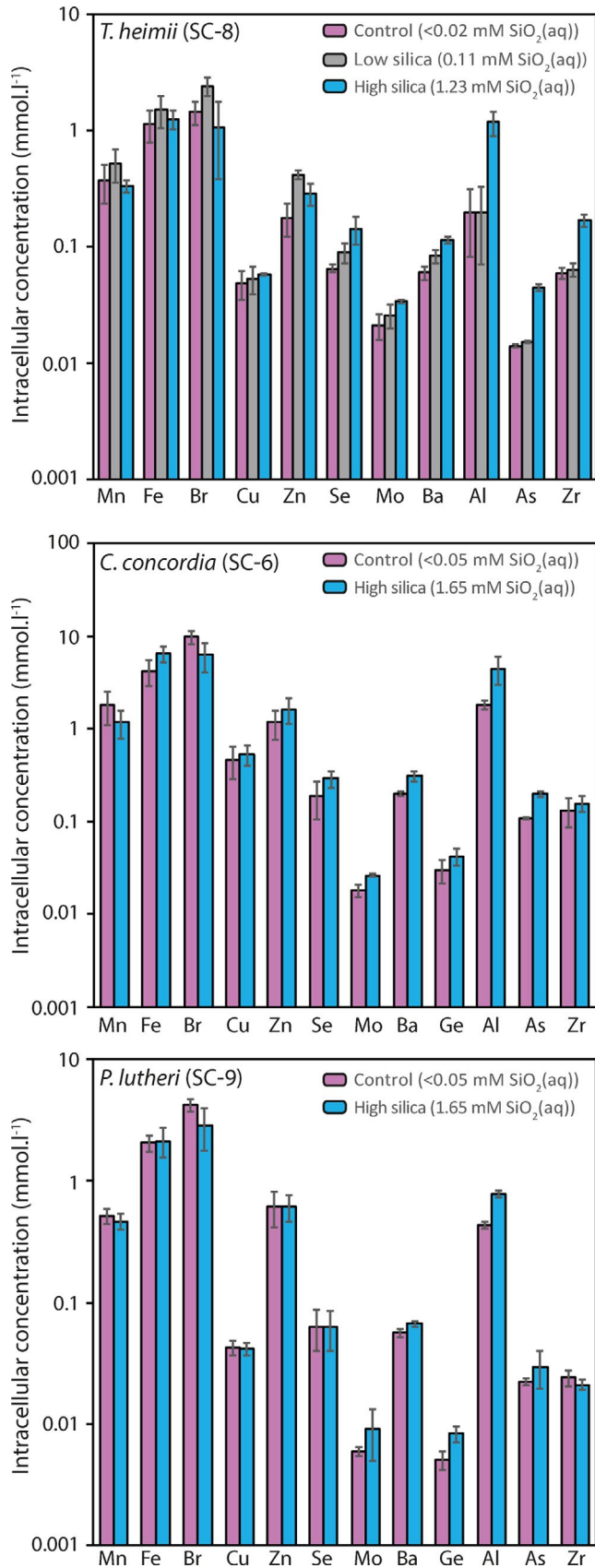


**FIGURE 3** Intracellular metal concentration for cells grown in control (pink), low silica (grey) and high silica media (blue). Each bar represents the average of triplicate cultures grown under identical conditions, and the error bar represents one standard deviation. SC = sub-culture

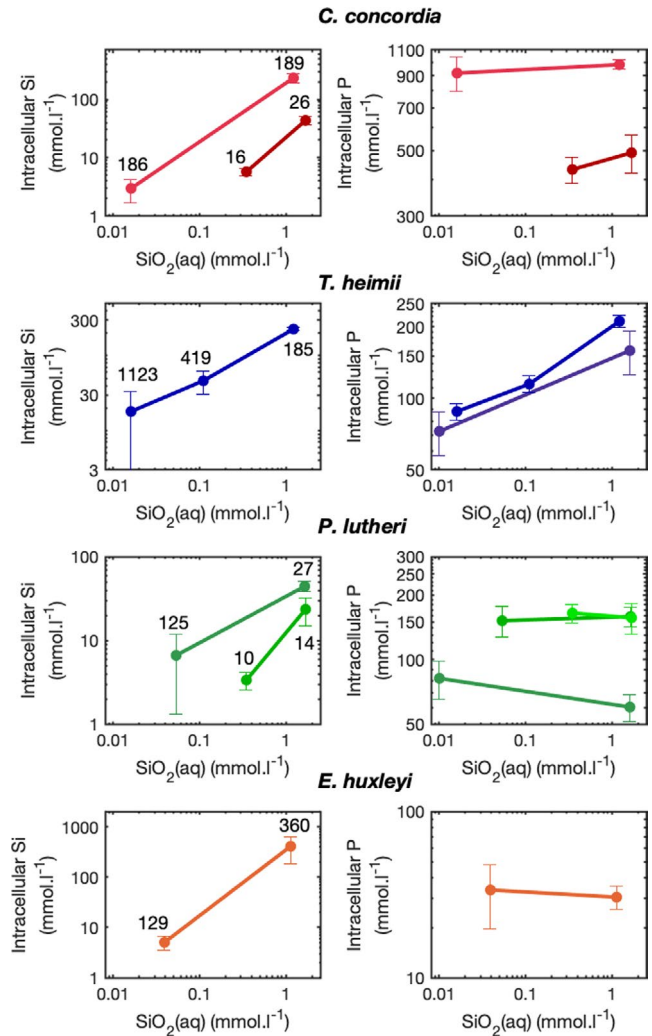


**FIGURE 4** Intracellular Si and P concentrations for each species compared with the Si concentration in the culture media. The intracellular concentrations were calculated from total digestions. Cell counts and cell diameters were calculated when cells were harvested. Each data point represents the average of triplicate cultures grown under identical conditions, and the error bar represents one standard deviation. Each coloured line represents cells harvested from independent sub-cultures. The ratio of intracellular Si to Si in the media (enrichment factor) is listed next to each data point. Note that the error associated with the calculated enrichment factor is larger when Si concentrations are lower

*Thoracosphaera heimii*, *E. huxleyi*, *C. concordia* and *P. lutheri* all accumulate intracellular silica at concentration orders of magnitude higher than the media, even under control conditions. All species show an increase in intracellular silica concentration when grown in silica-rich media compared with the control, and this is most pronounced in *T. heimii* and *E. huxleyi*, where intracellular silica concentrations exceed 200 mmol/L in Si-rich media (Figure 4). Enrichment factors (the ratio of silica in the cell to silica in the media) remain within an order of magnitude for most individual sub-cultures across a range of SiO<sub>2</sub>(aq), despite large variation between species and sub-cultures. *C. concordia* shows a different enrichment factor between

two sub-cultures, with lower intracellular Si when the cells were harvested later in exponential phase, suggesting that silica accumulation rates are highest at the start of exponential phase and decline during growth. For *T. heimii*, intracellular P concentrations also increased under silica-rich conditions (Figure 4).

### 3.3 | SEM data

During dinoflagellate cell division, the cell temporarily enters a resting stage, and then, the daughter cell emerges through the excystment opening. The excystment opening was clearly visible in around a third of calcified *T. heimii* cells grown under control conditions, but none were observed in cells grown under Si-rich conditions (Figure 6), despite observing >50 individual cells. Aside from this, there were no other observable differences in surface texture or morphology between cells grown under control and Si-rich conditions, including no evidence of extracellular  $\text{SiO}_2$  precipitates.

## 4 | DISCUSSION

### 4.1 | Eukaryotic stress in silica-rich seawater

All eukaryotic algae investigated here show potential signs of stress, including smaller cell size and/or reduced maximum growth rates under elevated  $\text{SiO}_2(aq)$ . This observation is consistent across the major eukaryotic lineages examined here, including algae from red and green lineages, and calcifying and non-calcifying red lineage algae. Relative to controls (i.e. no added  $\text{SiO}_2(aq)$ ), low concentrations of silica (up to 100  $\mu\text{mol/L}$ ) resulted in no discernible influence on growth rates, consistent with previous studies that tested silica levels between 1 and 100  $\mu\text{mol/L}$  (Fuhrman et al., 1978). However, silica appears to become detrimental to eukaryotic algae between 100  $\mu\text{mol/L}$  and 1 mmol/L, concentrations higher than any region of the modern ocean (<100  $\mu\text{mol/L}$  in deep waters, but as low as <0.2  $\mu\text{mol/L}$  in surface waters). Beyond these concentrations, increasing  $\text{SiO}_2$  (between 1.2 and 2.1 mmol/L) resulted in no discernible additional change in growth rates. In addition to changes in growth rate, all three algae from the red lineage show reduced cell sizes under high-Si treatment. Reduced cellular growth rate and/or cell size are common indicators of stress in algal culture. The absence of visible excystment openings in dinoflagellates grown under high-Si conditions is also consistent with slower cell division rates under stress. We will explore three possible mechanisms for inducing stress under high-Si conditions, including nutrient limitation, metal toxicity and the direct effects of intracellular Si accumulation.

### 4.2 | Nutrient limitation

Reduced growth rates are a common response to nutrient limitation. As we shall explore, nitrate limitation, rather than phosphate, is

more likely to be the principal driver when reduced growth rates are combined with reduced cell size. In the exponential growth phase, the mean diameter in a population of cells is controlled by the rate of nutrient assimilation into biomass and the time interval between cell division (i.e. the generation time) (Aloisi, 2015). In the assimilation phase of the cell cycle,  $\text{NO}_3^-$  consumption is higher as cells synthesise and accumulate biomass. Immediately before cell division, phosphate consumption is higher, as cells synthesise nucleic acids and membrane phospholipids. Therefore, phosphate limitation can arrest the cells in assimilation phase, causing them to bloat to larger sizes before each cell division. Given that two of the species exhibiting longer generation times (i.e. reduced growth rates) also exhibit reduced cell diameters, this is inconsistent with phosphate limitation. Further, the enhanced accumulation of P in *T. heimii* under silica-rich conditions is inconsistent with P limitation (Figure 4) and instead suggests *T. heimii* continues to accumulate P as some other factor limits growth rates. In contrast,  $\text{NO}_3^-$  limitation results in reduced cell diameter at each division and so could explain the combination of longer generation times and reduced cell diameter observed in *T. heimii* and *P. lutheri* in Si-rich seawater. This could occur if high  $\text{SiO}_2(aq)$  indirectly affects nitrate bioavailability in seawater, blocks nitrate uptake pathways or affects the availability of a micronutrient that plays a role in nitrate assimilation.

It is also possible that an alternative micronutrient is causing cell stress.  $\text{SiO}_2(aq)$  forms aqueous complexes with transition metals in seawater solutions that may alter their bioavailability, in particular if intracellular pH increases, as metal-silicate complex formation is strongly pH dependent (Choppin et al., 2011). One physiological response to nutrient limitation is to use an alternative pathway that depends on a different metal, but if a particular protein site depends on a single metal, an increase in the efficiency of metal uptake is required to maintain a requisite metabolic rate (Dupont et al., 2010). A reduction in cell diameter may balance this requirement, since this dramatically increases the surface area-to-volume ratio. The reduced cell sizes observed in all three algae from the red lineage may therefore be an expression of micronutrient limitation. Although the intracellular metal concentrations do not show a reduction under the high-Si treatment (Figure 3), metal limitation may not be expressed if the cells physiologically buffer the "free" metal availability with a storage strategy to maintain constant intracellular free levels. It is therefore difficult, at present, to identify the ultimate limiting nutrient from cell digests.

### 4.3 | Metal toxicity

Our data suggest that cellular metal quotas increase for some metals in the high-Si treatment. These are largely metals with no known biological role, including As, Al and Ge, but also Mo, which is required by all microbes. Assuming these metal quotas represent intracellular accumulation, as opposed to adsorption or precipitation on the surface of the cell, they could be a symptom of cell stress: if a critical metal is limited, the stressed algae

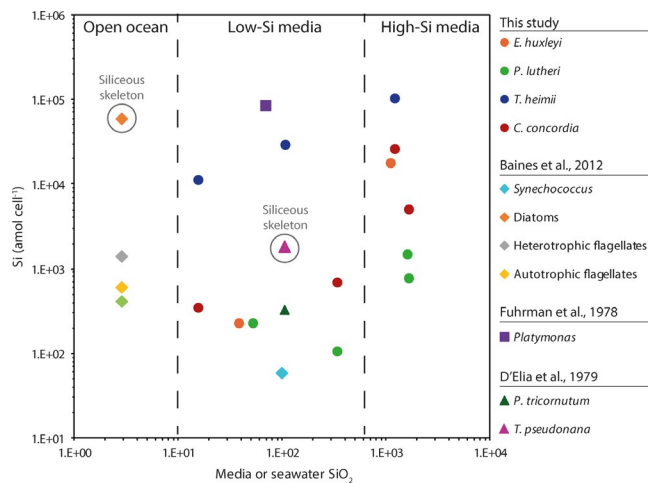


**FIGURE 5** Intracellular silica concentration, in amol. per cell, for a range of algal species with no known silica requirement. Data are from Baines et al. (2012) (diamonds); Fuhrman et al. (1978) (square); D'Elia et al. (1979) (triangles); and this study (circles). Cells from the open ocean come from equatorial upwelling regions of the Pacific Ocean

may respond by indiscriminately taking up other metals from seawater. Alternatively, metalloid accumulation could be a driver of cell stress, if increased metal accumulation is inadvertent. This could occur if the metals are complexed with Si as it enters the cell. Aluminium, for example, forms particularly strong complexes with Si. Some Si-specific transporters (e.g. *LiS2*) can also transport metalloids, such as arsenic (Ma et al., 2008) or germanium (Durak et al., 2016). Another possibility is that the cells could lose the ability to remove toxic metals under high-Si conditions. The high concentration of Si may compete with metals such as Ge and Al at the efflux pump due to molecular mimicry, causing build-up of these metals within the cell (Thamatrakoln & Hildebrand, 2008). Metalloids may also become trapped inside the cell complexed together with the Si, either within metalloid-Si complexes or as an impurity in silicate minerals. Regardless of the accumulation mechanism, high metalloid contents are a sign of stress and could result in intracellular metal toxicity.

#### 4.4 | Intracellular silica accumulation

Free Si in the cytoplasm has the potential to disrupt cellular metabolism by, for example, binding to proteins (Bienert et al., 2008; Martin-Jézéquel et al., 2000). The eukaryote species tested here were all found to accumulate intracellular silica in the control ranging from 3 to 17 mmol/L. Intracellular  $\text{SiO}_2$  accumulation in eukaryotes appears to scale with the  $\text{SiO}_2$  concentration in the media. Therefore, in the high- $\text{SiO}_2$  treatment, intracellular  $\text{SiO}_2$  levels were much higher, ranging from ~20 mmol/L in *P. lutheri* to ~400 mmol/L in *E. huxleyi*. Silica begins to auto-polymerise at concentrations  $>2$  mmol/L under circumneutral pH (Iler, 1979), and so these intracellular silica concentrations range up to 200 times above silica saturation (Siever, 1962;

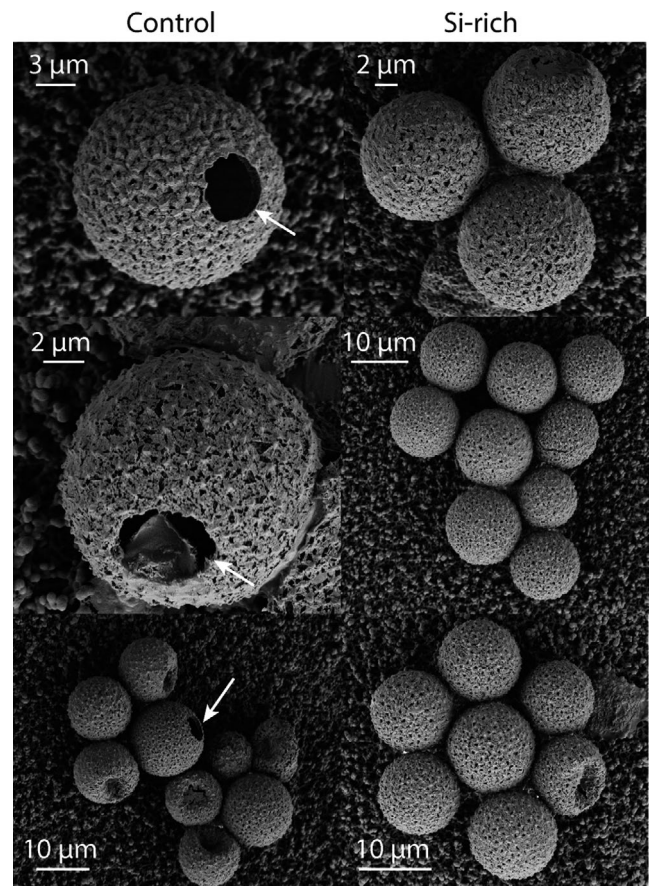


**FIGURE 6** SEM images of *T. heimii* grown under control conditions (left) and in high-silica media (right). Note the clear excystment opening under control conditions (white arrows)

Siever & Woodford, 1973). This phenomenon has been noted previously in microbes including *Synechococcus sp.*, *Platymonas sp.* and *Phaeodactylum tricornutum* (Baines et al., 2012; Brzezinski et al., 2017; Fuhrman et al., 1978; Nelson et al., 1984), and the intracellular  $\text{SiO}_2$  concentrations fall within a similar range, despite a range of culturing and  $\text{SiO}_2$  analysis techniques, suggesting intracellular silica accumulation is widespread among non-silicifying microbes (Figure 5).

One concern is that the bulk cellular digests included inorganic phases such as Mg-silicates that precipitated on cell surfaces or as an independent phase in the media and were not removed during washing. Mg-silicate precipitation is favoured at higher pH ( $>8.5$ ) (Tutolo & Tosca, 2018). Although the media was set to pH 8.1–8.2 before inoculation, pH can increase in dense batch cultures due to photosynthetic  $\text{CO}_2$  uptake, potentially reaching pH  $>8.5$  (Nelson et al., 1984). However, several observations rule out inorganic Mg-silicate contributions to our bulk digests. First, apparent silica uptake in *C. concordia* is higher in the early stages of exponential phase, when the pH change is likely to be small (Figure 4). Second, silica accumulation is observed in both calcifying and non-calcifying species, despite calcification driving a decrease in pH throughout growth that could counterbalance the pH increase driven by photosynthesis (Nimer et al., 1994). We confirmed that the pH remained within



**TABLE 3** Summary of response to silica-rich seawater compared to a control. Presence or absence of silica-specific transporters as reported in Durak et al. (2016) and Marron et al. (2016)

Species	Lineage	Calcifying?	Silicon transporters	Growth rates under high-Si treatment c.f. control	Cell diameter under high-Si treatment c.f. control	Intracellular metal content under high-Si treatment c.f. control
Eukaryotes						
<i>E. huxleyi</i>	Red	Yes	Lsi2-like	Same	Lower	No data
<i>T. heimii</i>	Red	Yes	Unknown, but other dinoflagellates have SIT-L & Lsi2-like.	Lower	Lower	Increase in Se, Mo, Ba, As, Al, Zr
<i>C. concordia</i>	Green	No	Unknown, but closely related <i>C. reinhardtii</i> has none.	Lower	Same	Increase in Mo, Ba, Al and As
<i>P. lutheri</i>	Red	No	None reported	Lower	Lower	Increase in Al and Ge
Prokaryote						
<i>Synechococcus</i> sp.	N/A	No	SIT-L	Same	No data	No data

range of a sterile control during early to mid-exponential phase for both *T. heimii* and *E. huxleyi* in silica-rich media (figure S7). Since we harvested cells in mid-exponential phase, this rules out the possibility of pH-induced precipitation in these cultures. Third, the cells were soaked three times in SOW with a pH of 8 for >20 min prior to digestion, which should have dissolved any inorganic Mg-silicates (Nelson et al., 1984). Therefore, our data support true intra- or extra-cellular organic uptake/absorption of silica by all four species, consistent with previous reports of intracellular silica accumulation in non-silicifying microbes at similar levels (Figure 5; Baines et al., 2012; Brzezinski et al., 2017; D'Elia et al., 1979; Fuhrman et al., 1978).

What form does this cellular silica take? One possibility is that silicate minerals were deposited external to the cell wall. However, no evidence for this was observed with our SEM images of *T. heimii*, in cells associated with significant Si accumulation (Figure 6). Observations of intracellular silica accumulation in the open ocean, where ambient  $\text{SiO}_2(\text{aq})$  is undersaturated with respect to silicate minerals, further supports a true intracellular form (Baines et al., 2012). If the  $\text{SiO}_2$  present in bulk cell digests is truly intracellular, it is possible that silicate minerals are precipitating inside the cell, contained within membrane-bound vacuoles, although no such vacuoles have been observed in diatom studies (Rogerson et al., 1987). An alternative possibility for maintaining such high intracellular silica concentrations is the presence of organic complexes inside the cell that bind to silica and increase its solubility (Hildebrand, 2000; Hildebrand & Wetherbee, 2003; Martin-Jézéquel et al., 2000). There is currently no direct evidence for such complexes existing outside of diatoms, and they remain poorly characterised (Azam, 1974; Baines et al., 2012; Bhattacharyya & Volcani, 1983; Hildebrand, 2000; Sullivan, 1979).

Such high intracellular silica concentrations raise the question of how silica is entering and being retained within the cell. If silica is acting as a nutrient, then it may be entering the cell via active uptake. The algae tested here have no known Si requirement. However, active Si uptake may be a strategy to lower local seawater Si to inhibit silica-dependent competitors (Fuhrman et al., 1978), and small amounts of silica have been shown to play an indirect role in other processes, such as coccolith formation (Durak et al., 2016). Active transport of Si into and around the cell could be facilitated by silica specific transporters, such as the SITs, a gene family first characterised in diatoms that facilitate  $\text{Na}^+$  coupled transport of silicic acid (Hildebrand et al., 1997). In diatoms, SITs are required to move Si around the cell to the silica depositional vesicle without inducing polymerisation. Recent work has found that silica transporters (including SITs, SIT-Ls and Lsi2) are present across a broad range of species from disparate lineages, including non-silicifying taxa, and appear to have a common origin (Durak et al., 2016; Marron et al., 2016). If algae have a form of Si importer that is constitutively expressed, and no regulatory pathway to switch the transporter off in high-silica environments, then in the absence of an independent and efficient efflux pathway, cells could continue to accumulate intracellular silica.

However, Si accumulation and signs of stress occur in species both with and without known Si transporters (Table 3). *E. huxleyi* has Lsi2-like

Si transporters, and *Synechococcus* possesses SIT-L genes (Marron et al., 2016). Some dinoflagellates have SIT-L and Lsi2 transporters, but phylogenetic analysis is required to confirm whether they are also present in *T. heimii*. In contrast, the presence of Si transporters in *C. reinhardtii* and *P. lutheri* is not documented. Thus, even species with Si transporters, which may help safely transport silica around the cell, are overloaded when  $\text{SiO}_2(aq)$  reaches Precambrian levels ( $>1$  mmol/L). This is consistent with the high binding affinity for SITs ( $K_D = 2.9$   $\mu\text{M}$ ) (Knight et al., 2016). The presence of high intracellular silica levels in species without known Si transporters suggests that Si uptake may not be exclusively occurring via Si-specific transporters. Further, it suggests that the presence of Si transporters is not able to regulate intracellular Si accumulation through increased efflux, either because they are not adapted for efflux in extant species, or because the efflux pathways are also overwhelmed at such high ambient  $\text{SiO}_2(aq)$ .

Another possibility is that active uptake is occurring mistakenly, via transporters intended for other ions. This could result in nutrient starvation if Si interferes with the uptake efficiency of other transporters. Alternatively, uncharged forms of silica may be entering the cell via diffusion. There appears to be a species-specific proportional relationship between intracellular  $\text{SiO}_2$  levels and the concentration of  $\text{SiO}_2$  in the media, suggesting they have very little control over uptake, consistent with diffusion (Figure 4). Diffusion could continue across the cell wall, despite intracellular concentrations exceeding ambient marine  $\text{SiO}_2(aq)$ , if organic complexes are present that bind to intracellular silica, increasing its solubility (Thamatrakoln & Hildebrand, 2008).

#### 4.5 | Response of eukaryotic algae versus cyanobacteria

The cyanobacteria *Synechococcus* does not show a detrimental response to high Si conditions, raising the possibility that prokaryotes are better equipped to deal with elevated silica than eukaryotic algae. Cyanobacteria employ a strategy centred around nutrient acquisition and efflux, by encoding a significantly greater proportion of transporting families (~2.8%) in the proteome compared with eukaryotes (0.5 to 1%) (Zhang et al., 2018). Essentially, they are high flow-through cells that invest less energy in nutrient storage and do not form Si-binding phytochelatins. This may result in a better ability for nutrient acquisition and efflux that helps them deal with high-Si conditions. Another potential mechanism to reconcile the differential impact of high-Si conditions on cyanobacteria and eukaryotic algae is if high-Si conditions result in Zn and Cu limitation, since eukaryotes have particularly high requirements for these two metals compared to the prokaryotes (Williams & Rickaby, 2012). At high intracellular  $\text{SiO}_2(aq)$  concentrations, Zn and Cu may be complexed with aqueous  $\text{SiO}_2$ , or precipitate as Zn-silicate or Cu-silicate minerals. Available geochemical data suggest that precipitation of Zn- and Cu-silicate minerals should proceed at near-neutral pH under the intracellular  $\text{SiO}_2$  concentrations observed here (Tiller & Pickering, 1974; Yates et al., 1998).

#### 4.6 | Early eukaryotes, intracellular $\text{SiO}_2(aq)$ uptake and Precambrian $\text{SiO}_2(aq)$ levels

The first unambiguous eukaryotic fossils are found in the late Palaeoproterozoic Era ( $>1.65$  Ga), but eukaryotes remained ecologically marginalised throughout the Mesoproterozoic (Butterfield, 2015; Javaux, 2007; Javaux & Knoll, 2017; Javaux et al., 2001; Javaux & Lepot, 2018). Recent data indicate that eukaryotic microfossils increase in taxonomic richness during and after the ~800–780 Ma Bitter Springs Event, but this metric progressively decreases leading up to the ~717 Ma onset of the Sturtian glaciation (Cohen & Riedman, 2018; Riedman & Sadler, 2018). Biomarker data have been interpreted to reflect a rise to ecological dominance in the aftermath of the Sturtian glaciation, at which point eukaryotic contributions to organic carbon remain significant through much of the remaining Neoproterozoic (Figure 1) (Brocks et al., 2017; Cohen & Macdonald, 2015). From one perspective, these data indicate that early eukaryotic diversification took place in oceans that featured higher levels of  $\text{SiO}_2(aq)$  than today, simply because these evolutionary events pre-date the radiation of siliceous skeletons in the Phanerozoic (Siever, 1992; Sperling et al., 2010). At the same time, our culturing data suggest that elevated  $\text{SiO}_2(aq)$  levels have a negative physiological effect on a range of extant eukaryotes. Did marine  $\text{SiO}_2(aq)$  levels influence Proterozoic eukaryotic ecosystems, and if so, how?

Although Si transporters currently play a role in uptake and transport across many eukaryote species, it has been proposed that the original role of Si transporters was for silica detoxification in high-Si Precambrian oceans (Marron et al., 2016). In the early Palaeozoic, these transporters may have been adapted for biosilicification as part of an evolutionary arms race that included the appearance of biominerals made from carbonate, phosphate and silicate minerals (Marin et al., 1996). This in turn reduced ambient marine  $\text{SiO}_2(aq)$  levels (Maliva et al., 1989), driving widespread loss or transformation of Si transporters in non-silicifying species (Marron et al., 2016). This hypothesis implies that in Precambrian oceans, microbes would have had biochemical machinery to deal with elevated marine  $\text{SiO}_2(aq)$ . In contrast, our results suggest that where Si transporters were retained, those species still struggle to deal with elevated  $\text{SiO}_2(aq)$  ( $>1$  mmol/L). However, this may simply indicate that Si transporters in extant organisms have been adapted to new conditions, by changing their role or binding affinity and can no longer act as efficient efflux pumps under very high  $\text{SiO}_2(aq)$ . If early eukaryotes did lack specialist adaptations to cope with elevated  $\text{SiO}_2(aq)$ , then the abundance of diverse eukaryotes in late Proterozoic ecosystems could indicate that  $\text{SiO}_2(aq)$  was lower or more variable than commonly thought.

A critical issue in determining how marine  $\text{SiO}_2(aq)$  levels influenced early eukaryotic ecosystems is to what extent the record of syndimentary and early diagenetic chert actually constrains marine  $\text{SiO}_2(aq)$  concentrations. Although primary silica grains characterise many Archaean and Palaeoproterozoic successions, evidence for direct amorphous silica primary precipitation from

the water column in the later Proterozoic is in fact more limited. Silica-rich granules clearly attest to spontaneous precipitation of amorphous  $\text{SiO}_2$  from the water column in the Archaean, indicating that seawater occasionally crossed solubility requirements, perhaps with the help of salinity fluctuations (Stefurak et al., 2014, 2015). Similarly, many silica-rich facies within banded iron formations contain evidence for primary or early diagenetic silica precipitation in subtidal environments (Maliva et al., 2005; Rasmussen et al., 2015). In contrast, most early diagenetic chert of late Proterozoic age formed in peritidal settings and is petrographically distinct in comparison (Fairchild et al., 1991; Hofmann, 1976; Knoll, 1982; Knoll et al., 1991; Muir, 1976; Schopf, 1968; Sergeev et al., 1995, 1997). For example, early silicification of carbonate-rich lithologies includes permineralisation of organic matter, chalcidonic cements, micro-quartz precipitation as carbonate minerals were replaced, and mosaics of larger interlocking quartz crystals somewhat similar to “mesoquartz” produced from modern silica sinters (Green et al., 1989; Knoll, 1985; Knoll & Simonson, 1981; Maliva et al., 1989, 2005).

Although permineralisation must have occurred very soon after organic material entered the sediments (i.e. before complete degradation), the marine  $\text{SiO}_2(aq)$  concentrations required to drive this process are poorly constrained. On the basis of sedimentological and stratigraphic constraints, many authors have suggested that evaporation in peritidal settings assisted in driving early silicification (Fairchild et al., 1991). Because early diagenetic silicification is comparatively rare in sediments today, these data imply elevated  $\text{SiO}_2(aq)$  levels compared with the modern ocean. This inference is also supported by recent experimental data showing that the formation and subsequent breakdown of aqueous organo-silica complexes facilitates high supersaturation and rapid nucleation of amorphous silica from seawater-like solutions (Escario Perez et al., 2020). Nevertheless,  $\text{SiO}_2(aq)$  could potentially have been below amorphous silica saturation, or even cristobalite saturation, through much of the late Proterozoic. In fact, mass balance modeling of the chert-hosted  $\delta^{30}\text{Si}$  record suggests that marine  $\text{SiO}_2(aq)$  might have decreased through the later portion of the Proterozoic compared to earlier intervals (Figure 1; Trower & Fischer, 2019), possibly driven by increases in authigenic clay formation (Isson & Planavsky, 2018). Thus, disentangling the relationship between early eukaryotic evolution and the history of marine  $\text{SiO}_2(aq)$  requires improved and more quantitative estimates of marine  $\text{SiO}_2(aq)$  through time, and a more complete understanding of the physiological mechanisms underpinning metabolic activities of early eukaryotes in  $\text{SiO}_2(aq)$ -rich seas.

## 5 | CONCLUSIONS

When exposed to Si-rich solutions that mimic Archaean–Proterozoic seawater, extant eukaryotic algae show signs of physiological stress. Under these conditions, eukaryotic algae accumulate intracellular silica, reaching concentrations far above the saturation state of

common silicate minerals, regardless of whether they possess silica-specific transporters. Such high levels of intracellular silica could interfere with normal cellular metabolism by, for example, chelating bioessential metals or trapping toxic metalloids. Early eukaryotes may have possessed modified Si transporters, designed to pump silica out of the cell, as an adaptation to Si-rich oceans. Alternatively, silica concentrations during early eukaryotic evolution may have been lower or more variable than commonly thought. One major outstanding question is why prokaryotes do not show signs of stress under elevated  $\text{SiO}_2(aq)$ , despite accumulating intracellular silica at comparable concentrations. This raises some interesting questions about the physiological mechanism underpinning the stress response in eukaryotes, with important implications for understanding the influence of declining  $\text{SiO}_2(aq)$  on early microbial evolution.

## ACKNOWLEDGEMENTS

Errin Johnson helped with SEM analysis and Phil Holdship assisted with ICP-MS analysis. Thank you to Sophie Gill, Roxana Shafiee, Ellen Cliff, Mahdi El Bendif, Samuel Eggins, and Steve Wyatt for help and advice in the laboratory. This work was supported by the NRF BIOGRIP platform, a NRF-DSI COE Palaeoscience grant to R Tostevin, ERC consolidator grant APPELS agreement number 681746 to R Rickaby and NERC grant NE/M013014/1 to N Tosca and R Rickaby. We thank two anonymous reviewers for thoughtful comments that helped to improve this manuscript.

## DATA AVAILABILITY STATEMENT

Data available in article supplementary material.

## ORCID

Rosalie Tostevin  <https://orcid.org/0000-0003-2843-7741>

## REFERENCES

- Aloisi, G. (2015). Covariation of metabolic rates and cell size in coccolithophores. *Biogeosciences*, 12, 6215–6284. <https://doi.org/10.5194/bg-12-4665-2015>
- Azam, F. (1974). Silicic-acid uptake in diatoms studied with  $[68\text{Ge}]$ germanic acid as tracer. *Planta*, 121, 205–212. <https://doi.org/10.1007/BF00389321>
- Baines, S. B., Twining, B. S., Brzezinski, M. A., Krause, J. W., Vogt, S., Assael, D., & McDaniel, H. (2012). Significant silicon accumulation by marine picocyanobacteria. *Nature Geoscience*, 5, 886–891. <https://doi.org/10.1038/ngeo1641>
- Bhattacharyya, P., & Volcani, B. E. (1983). Isolation of silicate ionophore(s) from the apochlorotic diatom *Nitzschia, alba*. *Biochemical and Biophysical Research Communications*, 114, 365–372. [https://doi.org/10.1016/0006-291X\(83\)91636-4](https://doi.org/10.1016/0006-291X(83)91636-4)
- Bienert, G. P., Schüssler, M. D., & Jahn, T. P. (2008). Metalloids: Essential, beneficial or toxic? Major intrinsic proteins sort it out. *Trends in Biochemical Sciences*, 33, 20–26. <https://doi.org/10.1016/j.tibs.2007.10.004>
- Brocks, J. J., Jarrett, A. J. M., Sirantoine, E., Hallmann, C., Hoshino, Y., & Liyanage, T. (2017). The rise of algae in Cryogenian oceans and the emergence of animals. *Nature*, 548, 578. <https://doi.org/10.1038/nature23457>
- Brzezinski, M. A., Krause, J. W., Baines, S. B., Collier, J. L., Ohnemus, D. C., & Twining, B. S. (2017). Patterns and regulation of silicon

- accumulation in *Synechococcus* spp. *Journal of Phycology*, 53, 746–761. <https://doi.org/10.1111/jpy.12545>
- Butterfield, N. J. (2015). Early evolution of the Eukaryota. *Palaeontology*, 58, 5–17. <https://doi.org/10.1111/pala.12139>
- Choppin, G. R., Pathak, P., & Thakur, P. (2011). Polymerization and complexation behavior of silicic acid: A review. *Main Group Metal Chemistry*, 31, 53–72. <https://doi.org/10.1515/MGMC.2008.31.1-2.53>
- Cohen, P. A., & Macdonald, F. A. (2015). The proterozoic record of eukaryotes. *Paleobiology*, 41, 610–632. <https://doi.org/10.1017/pab.2015.25>
- Cohen, P. A., & Riedman, L. A. (2018). It's a protist-eat-protist world: recalcitrance, predation, and evolution in the Tonian–Cryogenian ocean. *Emerging Topics in Life Sciences*, 2, 173–180. <https://doi.org/10.1042/ETLS20170145>
- Conley, D. J., Frings, P. J., Fontorbe, G., Clymans, W., Stadmark, J., Hendry, K. R., Marron, A. O., & De La Rocha, C. L. (2017). Biosilicification drives a decline of dissolved Si in the oceans through geologic time. *Frontiers in Marine Science*, 4, 397. <https://doi.org/10.3389/fmars.2017.00397>
- D'Elia, C. F., Guillard, R. R. L., & Nelson, D. M. (1979). Growth and competition of the marine diatoms *Phaeodactylum tricornutum* and *Thalassiosira pseudonana*. I. Nutrient effects. *Marine Biology*, 50, 305–312. <https://doi.org/10.1007/BF00387007>
- De Wever, P., O'dogherty, L., Caridroit, M., Dumitrica, P., Guex, J., Nigrini, C., & Caulet, J.-P. (2003). Diversity of radiolarian families through time. *Bulletin de la Société Géologique de France*, 174, 453–469. <https://doi.org/10.2113/174.5.453>
- Dupont, C. L., Butcher, A., Valas, R. E., Bourne, P. E., & Caetano-Anollés, G. (2010). History of biological metal utilization inferred through phylogenomic analysis of protein structures. *Proceedings of the National Academy of Sciences*, 107, 10567–10572. <https://doi.org/10.1073/pnas.0912491107>
- Durak, G. M., Taylor, A. R., Walker, C. E., Probert, I., de Vargas, C., Audic, S., Schroeder, D., Brownlee, C., & Wheeler, G. L. (2016). A role for diatom-like silicon transporters in calcifying coccolithophores. *Nature Communications*, 7, 10543. <https://doi.org/10.1038/ncomms10543>
- Egan, K. E., Rickaby, R. E. M., Hendry, K. R., & Halliday, A. N. (2013). Opening the gateways for diatoms primes Earth for Antarctic glaciation. *Earth and Planetary Science Letters*, 375, 34–43. <https://doi.org/10.1016/j.epsl.2013.04.030>
- Escario Perez, S., Nightingale, M., Humez, P., & Tutolo, B. M. (2020). The contribution of aqueous catechol-silica complexes to silicification during carbonate diagenesis. *Geochimica et Cosmochimica Acta*, 280, 185–201. <https://doi.org/10.1016/j.gca.2020.04.016>
- Fairchild, I. J., Knoll, A. H., & Swett, K. (1991). Coastal lithofacies and biofacies associated with syndepositional dolomitization and silicification (Draken Formation, Upper Riphean, Svalbard). *Precambrian Research*, 53, 165–197. [https://doi.org/10.1016/0301-9268\(91\)90071-H](https://doi.org/10.1016/0301-9268(91)90071-H)
- Fuhrman, J. A., Chisholm, S. W., & Guillard, R. R. L. (1978). Marine alga *Platymonas* sp. accumulates silicon without apparent requirement. *Nature*, 272, 244–246. <https://doi.org/10.1038/272244a0>
- Green, J. W., Knoll, A. H., & Swett, K. (1989). Microfossils from silicified stromatolitic carbonates of the Upper Proterozoic Limestone-Dolomite "Series", central East Greenland. *Geological Magazine*, 126, 567–585. <https://doi.org/10.1017/S0016756800022858>
- Hildebrand, M. (2000). Silicic Acid Transport and its Control During Cell Wall Silicification in Diatoms. *Biominer. Prog. Biol. Mol. Biol. Appl.*
- Hildebrand, M., Volcani, B. E., Gassmann, W., & Schroeder, J. I. (1997). A gene family of silicon transporters. *Nature*, 385, 688–689. <https://doi.org/10.1038/385688b0>
- Hildebrand, M., & Wetherbee, R. (2003). Components and control of silicification in diatoms. In W. E. G. Müller (Ed.), *Silicon Biomineralization: Biology – Biochemistry – Molecular Biology – Biotechnology, progress in molecular and subcellular biology* (pp. 11–57). Springer. [https://doi.org/10.1007/978-3-642-55486-5\\_2](https://doi.org/10.1007/978-3-642-55486-5_2)
- Hofmann, H. J. (1976). Precambrian Microflora, Belcher Islands, Canada: Significance and Systematics. *Journal of Paleontology*, 50, 1040–1073.
- Iler, K. (1979). The Chemistry of Silica. Solubility Polym. Colloid Surf. Prop. Biochem. Silica.
- Isson, T. T., & Planavsky, N. J. (2018). Reverse weathering as a long-term stabilizer of marine pH and planetary climate. *Nature*, 560, 471–475. <https://doi.org/10.1038/s41586-018-0408-4>
- Javaux, E. J. (2007). The early eukaryotic fossil record. In *Eukaryotic membranes and cytoskeleton: Origins and evolution, advances in experimental medicine and biology* (Vol. 607, pp. 1–19). New York, NY: Springer. [https://doi.org/10.1007/978-0-387-74021-8\\_1](https://doi.org/10.1007/978-0-387-74021-8_1)
- Javaux, E. J., & Knoll, A. H. (2017). Micropaleontology of the lower Mesoproterozoic Roper Group, Australia, and implications for early eukaryotic evolution. *Journal of Paleontology*, 91, 199–229. <https://doi.org/10.1017/jpa.2016.124>
- Javaux, E. J., Knoll, A. H., & Walter, M. R. (2001). Morphological and ecological complexity in early eukaryotic ecosystems. *Nature*, 412, 66–69. <https://doi.org/10.1038/35083562>
- Javaux, E. J., & Lepot, K. (2018). The Paleoproterozoic fossil record: Implications for the evolution of the biosphere during Earth's middle-age. *Earth Science Reviews*, 176, 68–86. <https://doi.org/10.1016/j.earscirev.2017.10.001>
- Kidder, D. L., & Mumma, S. A. (2003). Silica-replaced oolites, bedded shelf cherts and Paleozoic changes in the silica cycle. *Sedimentary Geology*, 162, 159–166. [https://doi.org/10.1016/S0037-0738\(03\)00195-7](https://doi.org/10.1016/S0037-0738(03)00195-7)
- Knight, M. J., Senior, L., Nancolas, B., Ratcliffe, S., & Curnow, P. (2016). Direct evidence of the molecular basis for biological silicon transport. *Nature Communications*, 7, 11926. <https://doi.org/10.1038/ncomms11926>
- Knoll, A. H. (1982). Microfossils from the late precambrian draken conglomerate, Ny Friesland, Svalbard. *Journal of Paleontology*, 56, 755–790.
- Knoll, A. H. (1985). Exceptional preservation of photosynthetic organisms in silicified carbonates and silicified peats. *Philosophical Transactions of the Royal Society B: Biological Science*, 311, 111–122. <https://doi.org/10.1098/rstb.1985.0143>
- Knoll, A. H., & Simonson, B. (1981). Early Proterozoic microfossils and penecontemporaneous quartz cementation in the Sokoman Iron Formation, Canada. *Science*, 211, 478–480. <https://doi.org/10.1126/science.211.4481.478>
- Knoll, A. H., Swett, K., & Mark, J. (1991). Paleobiology of a neoproterozoic tidal flat/lagoonal complex: The draken conglomerate formation. *Spitsbergen. J. Paleontol.*, 65, 531–570. <https://doi.org/10.1017/S0022336000030663>
- Ma, J. F., Yamaji, N., Mitani, N., Xu, X.-Y., Su, Y.-H., McGrath, S. P., & Zhao, F.-J. (2008). Transporters of arsenite in rice and their role in arsenic accumulation in rice grain. *Proceedings of the National Academy of Sciences*, 105, 9931–9935. <https://doi.org/10.1073/pnas.0802361105>
- Maliva, R. G., Knoll, A. H., & Siever, R. (1989). Secular change in chert distribution: A reflection of evolving biological participation in the silica cycle. *Palaios*, 4, 519–532. <https://doi.org/10.2307/3514743>
- Maliva, R. G., Knoll, A. H., & Simonson, B. M. (2005). Secular change in the Precambrian silica cycle: Insights from chert petrology. *Geological Society of America Bulletin*, 117, 835–845. <https://doi.org/10.1130/B25555.1>
- Marin, F., Smith, M., Isa, Y., Muyzer, G., & Westbroek, P. (1996). Skeletal matrices, muci, and the origin of invertebrate calcification. *Proceedings of the National Academy of Sciences USA*, 93, 1554–1559. <https://doi.org/10.1073/pnas.93.4.1554>
- Marron, A. O., Ratcliffe, S., Wheeler, G. L., Goldstein, R. E., King, N., Not, F., de Vargas, C., & Richter, D. J. (2016). The evolution of silicon

- transport in eukaryotes. *Molecular Biology and Evolution*, 33, 3226–3248. <https://doi.org/10.1093/molbev/msw209>
- Martin-Jézéquel, V., Hildebrand, M., & Brzezinski, M. A. (2000). Silicon metabolism in diatoms: Implications for growth. *Journal of Phycology*, 36, 821–840. <https://doi.org/10.1046/j.1529-8817.2000.00019.x>
- Muir, M. D. (1976). Proterozoic microfossils from the Amelia dolomite, McArthur Basin, Northern Territory. *Alcheringa: An Australasian Journal of Palaeontology*, 1, 143–158. <https://doi.org/10.1080/03115517608619066>
- Nelson, D. M., Riedel, G. F., Millan-Nunez, R., & Lara-Lara, J. R. (1984). Silicon uptake by algae with no known Si requirement. I. True cellular uptake and pH-induced precipitation by phaeodactylum tricornutum (bacillariophyceae) and platyomonas sp. (prasinophyceae)1. *Journal of Phycology*, 20, 141–147. <https://doi.org/10.1111/j.0022-3646.1984.00141.x>
- Nimer, N. A., Brownlee, C., & Merrett, M. J. (1994). Carbon dioxide availability, intracellular pH and growth rate of the coccolithophore *Emiliania huxleyi*. *Marine Ecology Progress Series*, 109, 257–262. <https://doi.org/10.3354/meps109257>
- Price, N. M., Harrison, G. I., Hering, J. G., Hudson, R. J., Nirel, P. M. V., Palenik, B., & Morel, F. M. M. (1989). Preparation and chemistry of the artificial algal culture Medium Aquil. *Biological Oceanography*, 6, 443–461. <https://doi.org/10.1080/01965581.1988.10749544>
- Quigg, A., Finkel, Z. V., Irwin, A. J., Rosenthal, Y., Ho, T.-Y., Reinfelder, J. R., Schofield, O., Morel, F. M. M., & Falkowski, P. G. (2003). The evolutionary inheritance of elemental stoichiometry in marine phytoplankton. *Nature*, 425, 291–294. <https://doi.org/10.1038/nature01953>
- Rasmussen, B., Krapež, B., & Muhling, J. R. (2015). Seafloor silicification and hardground development during deposition of 2.5 Ga banded iron formations. *Geology*, 43, 235–238. <https://doi.org/10.1130/G36363.1>
- Riedman, L. A., & Sadler, P. M. (2018). Global species richness record and biostratigraphic potential of early to middle Neoproterozoic eukaryote fossils. *Precambrian Res Descent into the Cryogenian*, 319, 6–18. <https://doi.org/10.1016/j.precamres.2017.10.008>
- Rogerson, A., DeFreitas, A. S. W., & McInnes, A. G. (1987). Cytoplasmic silicon in the centric diatom *Thalassiosira pseudonana* localized by electron spectroscopic imaging. *Canadian Journal of Microbiology*, 33, 128–131. <https://doi.org/10.1139/m87-022>
- Schopf, J. W. (1968). Microflora of the bitter springs formation, late precambrian, Central Australia. *Journal of Paleontology*, 42, 651–688.
- Sergeev, V. N., Knoll, A. H., & Grotzinger, J. P. (1995). Paleobiology of the mesoproterozoic billyakh group, anabar uplift, Northern Siberia. *Journal of Paleontology*, 69, 1–37. <https://doi.org/10.1017/S0022336000062375>
- Sergeev, V. N., Knoll, A. H., & Petrov, P. Y. (1997). Paleobiology of the mesoproterozoic-neoproterozoic transition: The sukhaya tunguska formation, Turukhansk Uplift, Siberia. *Precambrian Research*, 85, 201–239. [https://doi.org/10.1016/S0301-9268\(97\)00035-1](https://doi.org/10.1016/S0301-9268(97)00035-1)
- Siever, R. (1962). Silica solubility, 0°–200° C., and the diagenesis of siliceous sediments. *The Journal of Geology*, 70, 127–150. <https://doi.org/10.1086/626804>
- Siever, R. (1992). The silica cycle in the Precambrian. *Geochimica Et Cosmochimica Acta*, 56, 3265–3272. [https://doi.org/10.1016/0016-7037\(92\)90303-Z](https://doi.org/10.1016/0016-7037(92)90303-Z)
- Siever, R., & Woodford, N. (1973). Sorption of silica by clay minerals. *Geochimica Et Cosmochimica Acta*, 37, 1851–1880. [https://doi.org/10.1016/0016-7037\(73\)90146-4](https://doi.org/10.1016/0016-7037(73)90146-4)
- Sims, P. A., Mann, D. G., & Medlin, L. K. (2006). Evolution of the diatoms: Insights from fossil, biological and molecular data. *Phycologia*, 45, 361–402. <https://doi.org/10.2216/05-22.1>
- Sperling, E. A., Robinson, J. M., Pisani, D., & Peterson, K. J. (2010). Where's the glass? Biomarkers, molecular clocks, and microRNAs suggest a 200-Myr missing Precambrian fossil record of siliceous sponge spicules. *Geobiology*, 8, 24–36. <https://doi.org/10.1111/j.1472-4669.2009.00225.x>
- Stefurak, E. J. T., Lowe, D. R., Zentner, D., & Fischer, W. W. (2014). Primary silica granules—A new mode of Paleoproterozoic sedimentation. *Geology*, 42, 283–286. <https://doi.org/10.1130/G35187.1>
- Stefurak, E. J. T., Lowe, D. R., Zentner, D., & Fischer, W. W. (2015). Sedimentology and geochemistry of Archean silica granules. *Geological Society of America Bulletin*, 127, 1090–1107. <https://doi.org/10.1130/B31181.1>
- Sullivan, C. W. (1979). Diatom mineralization of silicic acid. IV. Kinetics of soluble Si pool formation in exponentially growing and synchronized *Navicula pelliculosa*. *Journal of Phycology*, 15(2), 210–216.
- Sunda, W. G., Price, N. M., & Morel, F. M. (2005). Trace metal ion buffers and their use in culture studies. *Algal Culturing Techniques*, 4, 35–63.
- Thamtrakoln, K., & Hildebrand, M. (2008). Silicon uptake in diatoms revisited: A model for saturable and nonsaturable uptake kinetics and the role of silicon transporters. *Plant Physiology*, 146, 1397–1407. <https://doi.org/10.1104/pp.107.107094>
- Tiller, K. G., & Pickering, J. G. (1974). The synthesis of Zinc silicates at 20°C and atmospheric pressure. *Clays and Clay Minerals*, 22, 409–416. <https://doi.org/10.1346/CCMN.1974.0220507>
- Trower, E. J., & Fischer, W. W. (2019). Precambrian Si isotope mass balance, weathering, and the significance of the authigenic clay silica sink. *Sedimentary Geology*, 384, 1–11. <https://doi.org/10.1016/j.sedgeo.2019.02.008>
- Tutolo, B. M., & Tosca, N. J. (2018). Experimental examination of the Mg-silicate-carbonate system at ambient temperature: Implications for alkaline chemical sedimentation and lacustrine carbonate formation. *Geochimica Et Cosmochimica Acta*, 225, 80–101. <https://doi.org/10.1016/j.gca.2018.01.019>
- Williams, R. J. P., & Rickaby, R. E. M. (2012). *Evolution's destiny: Co-evolving chemistry of the environment and life*. Royal Society of Chemistry.
- Wu, B., & Beitz, E. (2007). Aquaporins with selectivity for unconventional permeants. *Cellular and Molecular Life Sciences*, 64, 2413–2421. <https://doi.org/10.1007/s00018-007-7163-2>
- Yates, D. M., Joyce, K. J., & Heaney, P. J. (1998). Complexation of copper with polymeric silica in aqueous solution. *Applied Geochemistry*, 13, 235–241. [https://doi.org/10.1016/S0883-2927\(97\)00062-0](https://doi.org/10.1016/S0883-2927(97)00062-0)
- Zhang, Q., Nevado, B., Snow, J. T., Filatov, D., & Rickaby, R. E. M. (2018). The Mesozoic Marine Algal Revolution and trace metals: comparing metal acquisition strategies. AGU Fall Meet. Abstr. 33.
- Zhang, Q., Snow, J. T., Holdship, P., Price, D., & Watson, P. R. M. R. (2018). Direct measurement of multi-elements in high matrix samples with a flow injection ICP-MS: Application to the extended *Emiliania huxleyi* Redfield ratio. *Journal of Analytical Atomic Spectrometry*, 33, 1196–1208. <https://doi.org/10.1039/C8JA00031J>

## SUPPORTING INFORMATION

Additional supporting information may be found online in the Supporting Information section.

**How to cite this article:** Tostevin R, Snow JT, Zhang Q, Tosca NJ, Rickaby REM. The influence of elevated SiO<sub>2</sub>(aq) on intracellular silica uptake and microbial metabolism. *Geobiology*. 2021;00:1–13. <https://doi.org/10.1111/gbi.12442>